Supporting Information

5d → 4f Transition of Lanthanide-Activated MGa_2S_4 (M = Ca, Sr) Semiconductor for Mechanical-to-Light Energy Conversion Mediated by Structural Distortion

*Xianhui Zhang[a, b], Dong Yang[c], Shaofan Wu[a], Xieming Xu[a, b], Ronghua Ma[d], Dengfeng Peng[d, *], Zhilin Wang[a, b], and Shuaihua Wang[a, *]*

[a]Key Laboratory of Optoelectronic Materials Chemistry and Physics, Fujian Institute of Research on the Structure of Matter, Chinese Academy of Sciences, Fuzhou 350002, China

[b]University of the Chinese Academy of Sciences, Beijing 100049, China

[c]State Key Laboratory of New Ceramics and Fine Processing, School of Materials Science and Engineering, Tsinghua University

[d]Key Laboratory of Optoelectronic Devices and Systems of Ministry of Education and Guangdong Province, College of Optoelectronic Engineering, Shenzhen University, Shenzhen 518060, China

*Corresponding authors.
Email address: shwang@fjirsm.ac.cn (S.H. Wang), pengdengfeng@szu.edu.cn (D.F. Peng)

Table S1. Crystal Data and Structure Refinements of $CaGa_2S_4$ and $SrGa_2S_4$.

formula	$CaGa_2S_4$	$SrGa_2S_4$
fw(g/mol^{-1})	4924.16	5684.80
crystal system	Orthorhombic	Orthorhombic
space group	*Fddd* (No. 70)	*Fddd* (No. 70)
a (Å)	20.084(6)	20.8316(2)
b (Å)	20.046(6)	20.4949(2)
c (Å)	12.105(3)	12. 2090(1)
α (deg)	90	90
β (deg)	90	90
γ (deg)	90	90
V (Å^3)	4873.9(4)	5212.53(8)
Z	32	32
D_c (g·cm^{-3})	3.355	3.622
μ (mm^{-1})	10.911	20.767
GOOF on F^2	1.049	1.146
R_1, wR_2 ($I > 2\sigma(I)$)[a]	0.0325, 0.0954	0.0258, 0.0665

[a] $R_1 = \sum||F_o| - |F_c||/\sum|F_o|$, $wR_2 = [\sum w(F_o^2 - F_c^2)^2/\sum w(F_o^2)^2]^{1/2}$.

Table S2. The cell parameters of $CaGa_2S_4$ based models used in DFT calculation.

Parameters	Pure	Eu	Ce	Ce-Eu

a(Å)	14.2106	14.2112	14.2120	14.2116
b(Å)	11.7408	11.7410	11.7419	11.7415
c(Å)	11.7296	11.7300	11.7332	11.7318
α°	74.5252	74.5259	74.5280	74.5268
β°	52.7734	52.7740	52.7763	52.7749
γ°	52.7014	52.7028	52.7046	52.7037

Table S3. The experimental and optimized cell parameters, Bader charge analysis, bandgap of $CaGa_2S_4$ and $CaGa_2S_4$: Eu, and the optimized bond lengths of Ca–S/Eu–S at the Eu dope site.

Parameter	$CaGa_2S_4$(exp)		$CaGa_2S_4$(cal)		$CaGa_2S_4$:Eu(cal)	
a(Å)	12.1053		12.2273		12.2445	
b(Å)	20.0466		20.2573		20.3129	
c(Å)	20.0846		20.3207		20.4501	
α(°)	90		90		90	
β(°)	90		90		90	
γ(°)	90		90		90	
Bond(Ca/Eu–S) at dope	2.975	3.042	3.004	3.075	3.091	3.128
site(Å)	2.975	3.042	3.004	3.075	3.091	3.128
	2.975	3.042	3.004	3.075	3.091	3.128
	2.975	3.042	3.004	3.075	3.091	3.128
Bader charge analysis of Eu					–1.47e	
Bandgap(eV)			2.79		2.57	
Minimum direct bandgap			2.86		2.59	

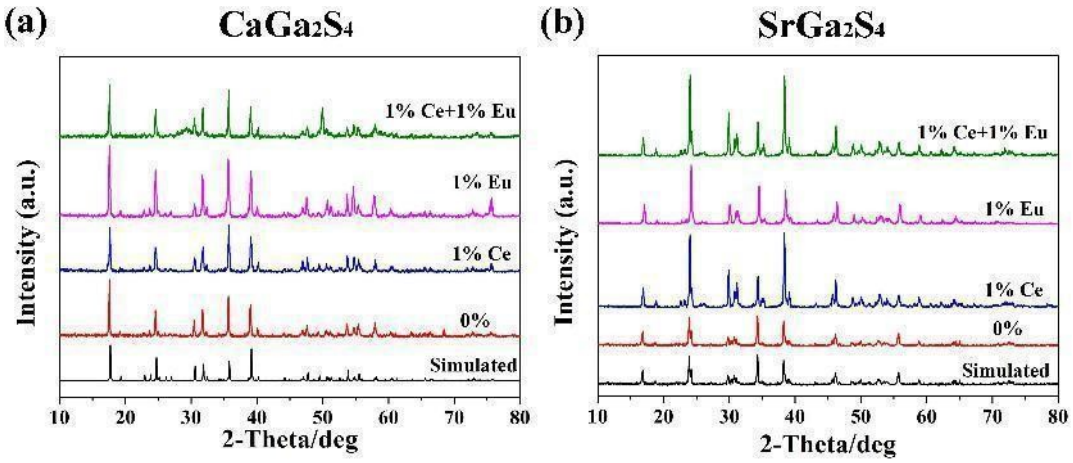

Fig. S1. PXRD patterns of the lanthanides-doped (a) $CaGa_2S_4$ and (b) $SrGa_2S_4$, respectively.

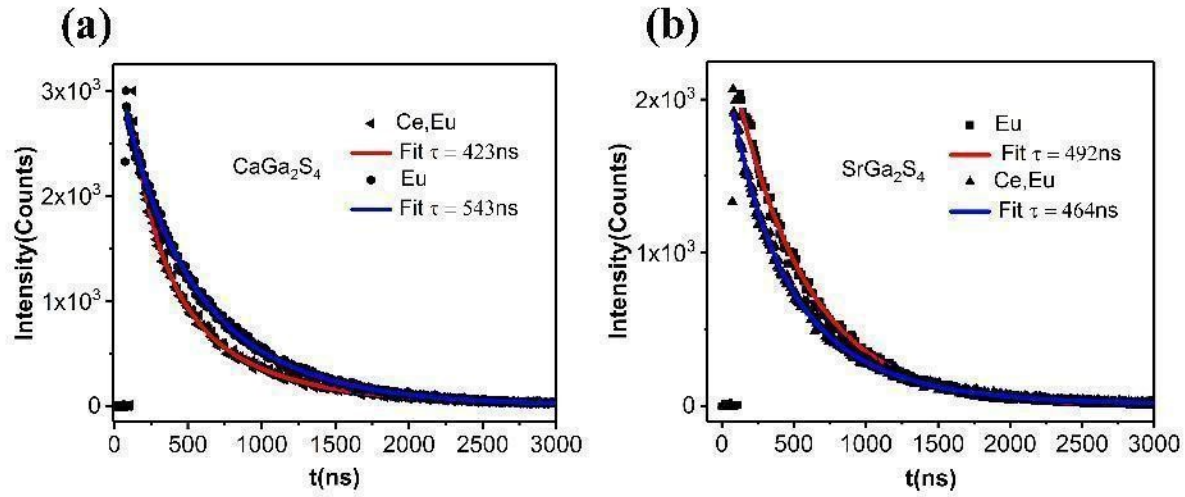

Fig. S2. The fluorescence decay curves of the Eu, Ce-Eu activated (a) $CaGa_2S_4$ and (b) $SrGa_2S_4$, respectively.

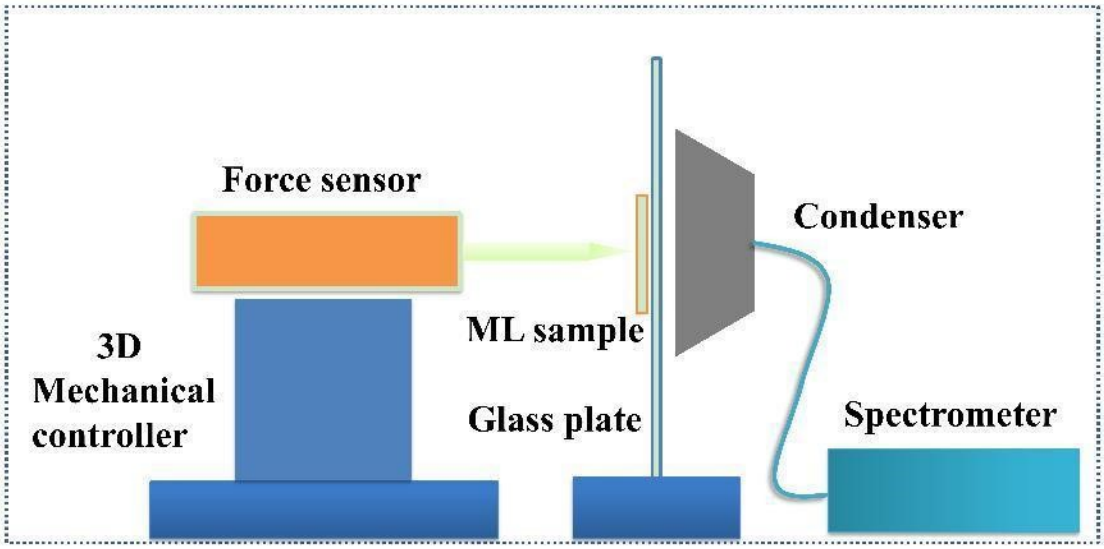

Fig. S3. Schematic diagram of the equipment for ML test.

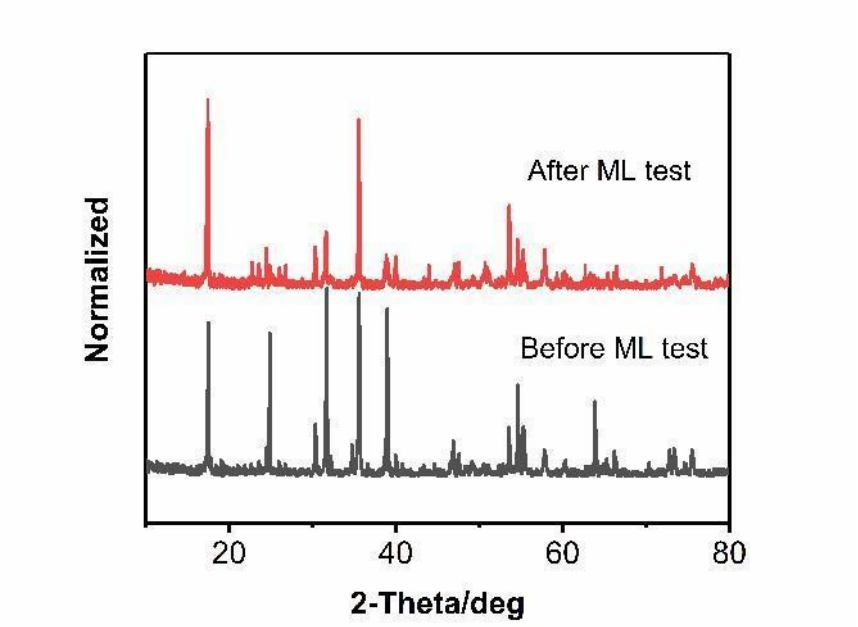

Fig. S4. PXRD of the $CaGa_2S_4$: Ce, Eu crystal samples before and after ML test.

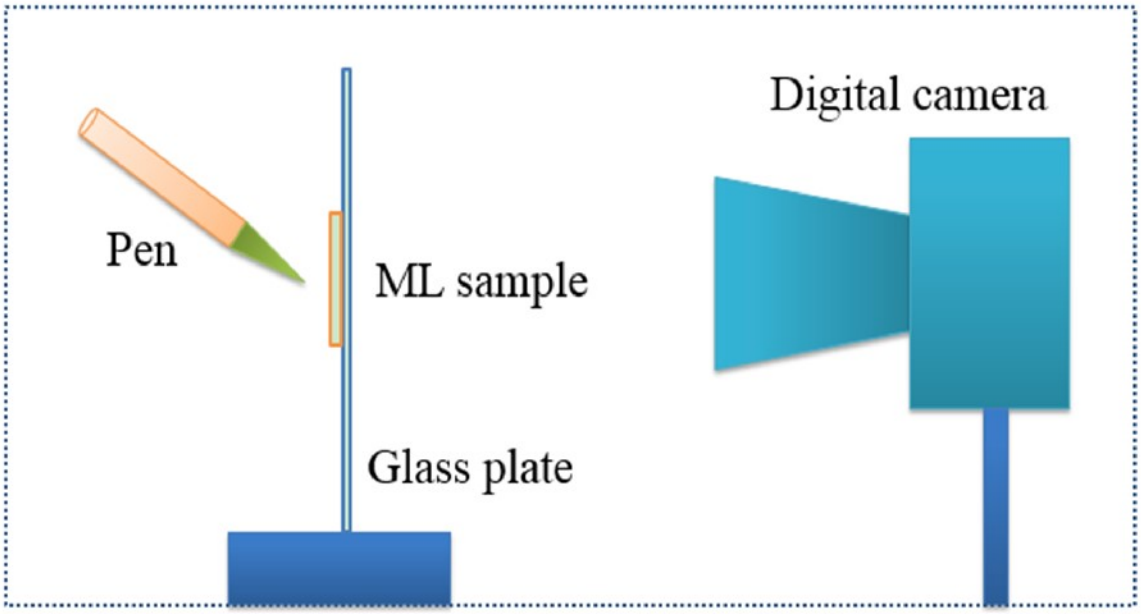

Fig. S5. Simplified diagram of signal acquisition of the self-powered display.

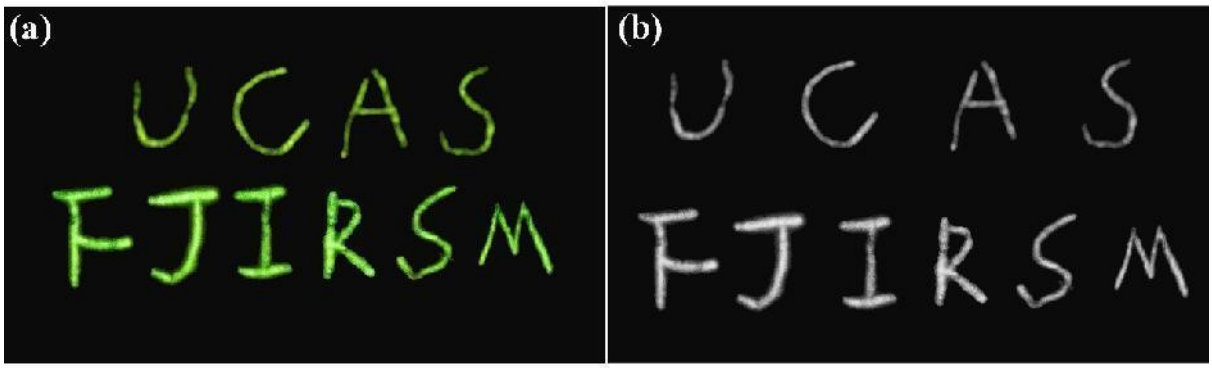

Fig. S6. (a) 2D planner pressure map and (b) extracted gray picture of the ML photograph captured from a handwritten letter "UCAS" and "FJIRSM" from the ML film sample.

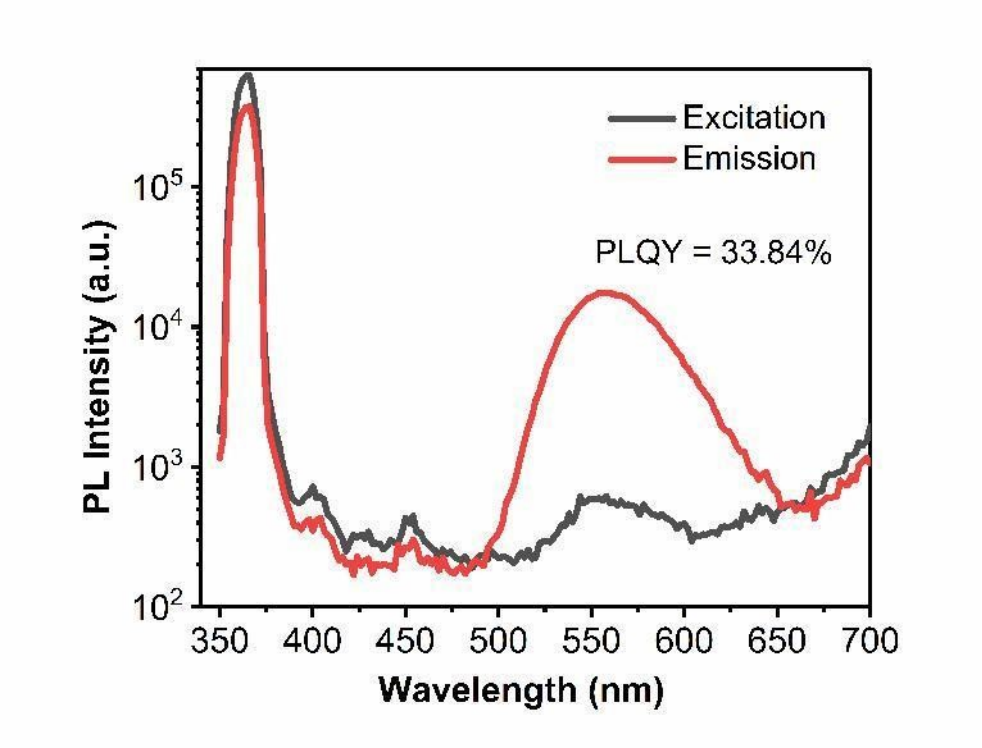

Fig. S7. The excitation and emission spectrum of $CaGa_2S_4$: Ce, Eu and the excitation calibration curve without sample for PLQY calculation collected by an integrating sphere under excitation light at 360 nm.

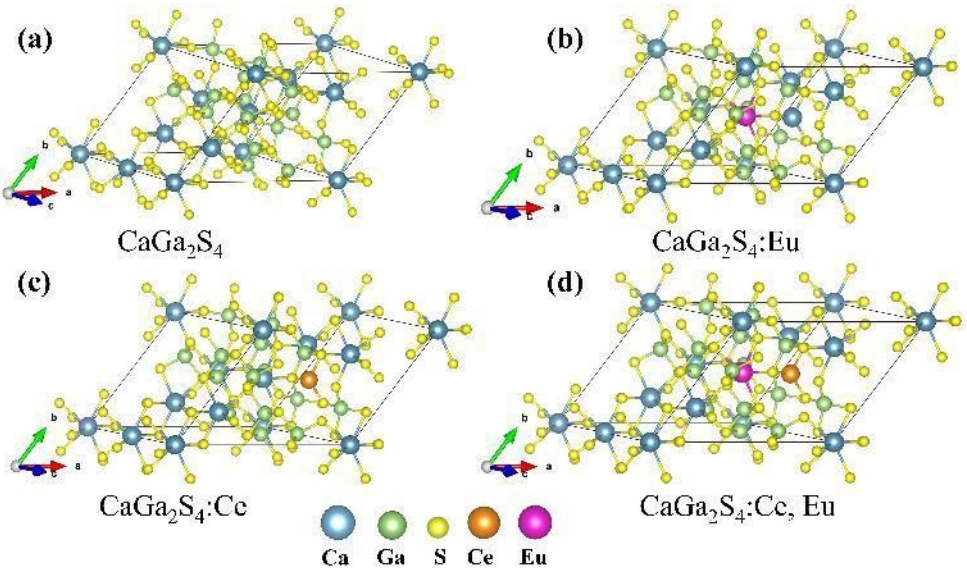

Fig. S8. The four optimized models of (a) $CaGa_2S_4$, (b) $CaGa_2S_4$: Eu, (c) $CaGa_2S_4$: Ce and (d) $CaGa_2S_4$: Ce, Eu in which the dope concentrations of the activators are 0.0305, 0.0305 and 0.061,

namely, the formula can be written as $Ca_{0.9695}Eu_{0.0305}Ga_2S_4$, $Ca_{0.9695}Ce_{0.0305}Ga_2S_4$, $Ca_{0.9695}(Ce, Eu)_{0.061}Ga_2S_4$, respectively.

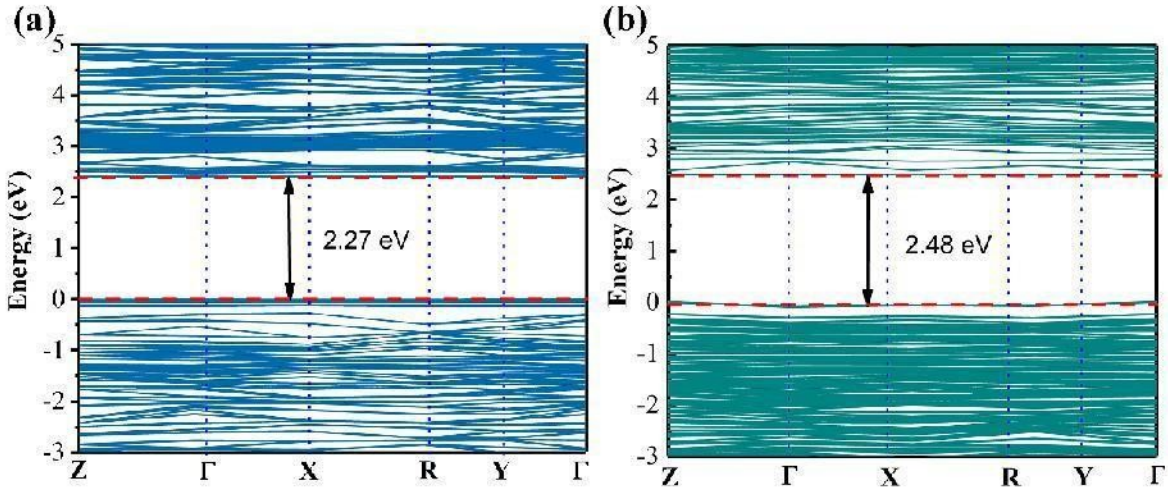

Fig. S9. The band structures of (a) $CaGa_2S_4$: Eu and (b) $CaGa_2S_4$: Ce, represented by sky blue and dark green line.

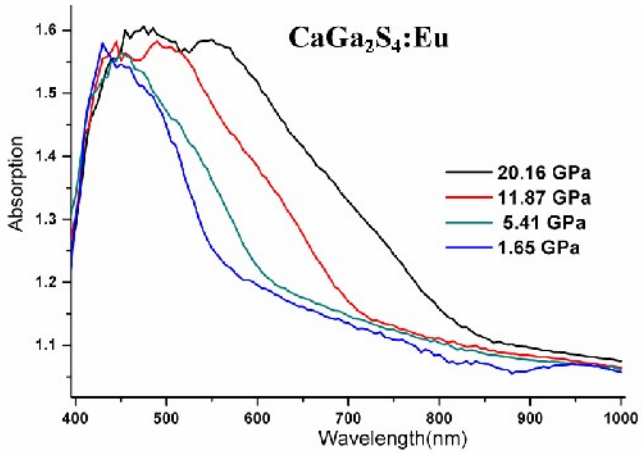

Fig. S10. Absorption spectrum of the $CaGa_2S_4$: Eu crystals under different high pressures (1.65 GPa, 5.41 GPa, 11.87 GPa and 20.16 GPa).

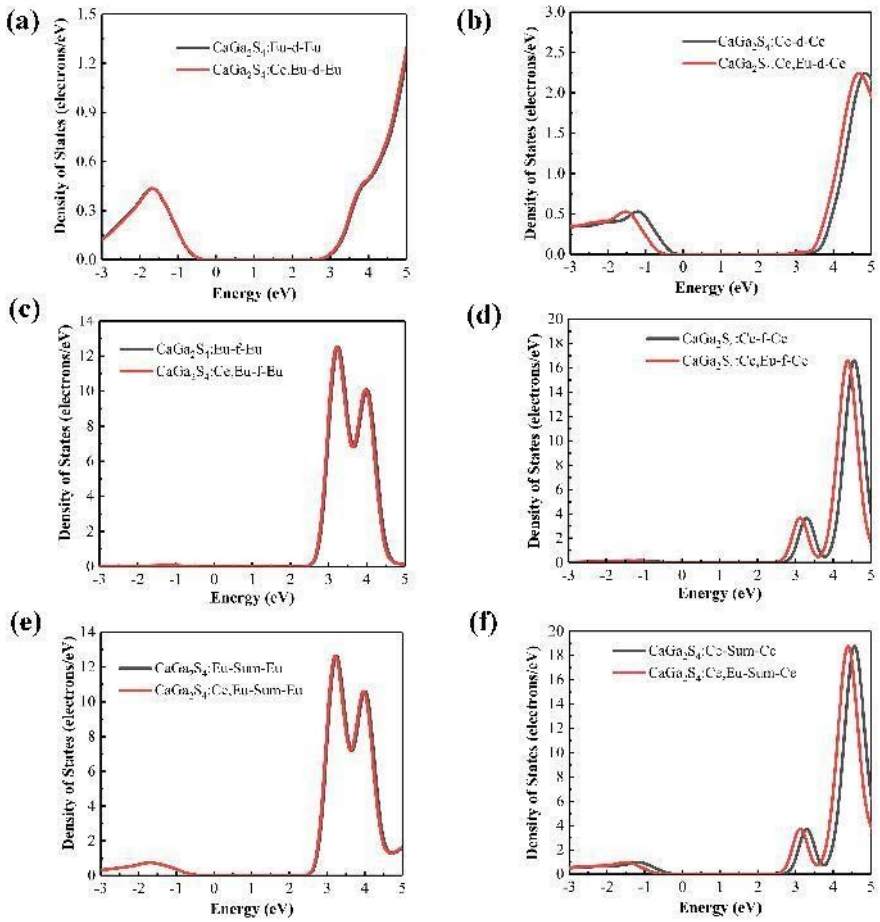

Fig. S11. The corresponding PDOS (d and f orbitals of lanthanides) (a-d) and DOS (s, p, d, f orbitals Sum of lanthanides) (e-f) of the Eu, Ce and Ce–Eu doped host $CaGa_2S_4$.

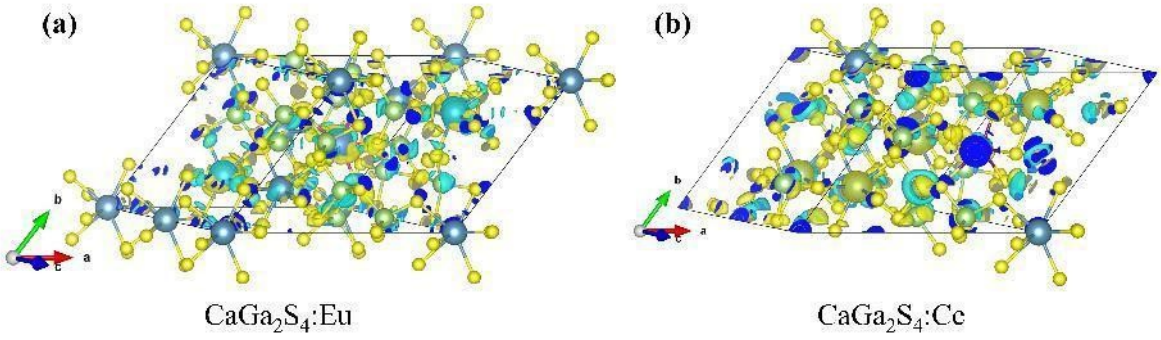

Fig. S12. The difference charge density diagrams with respect to (a) $CaGa_2S_4$: Eu and (b) $CaGa_2S_4$: Ce.

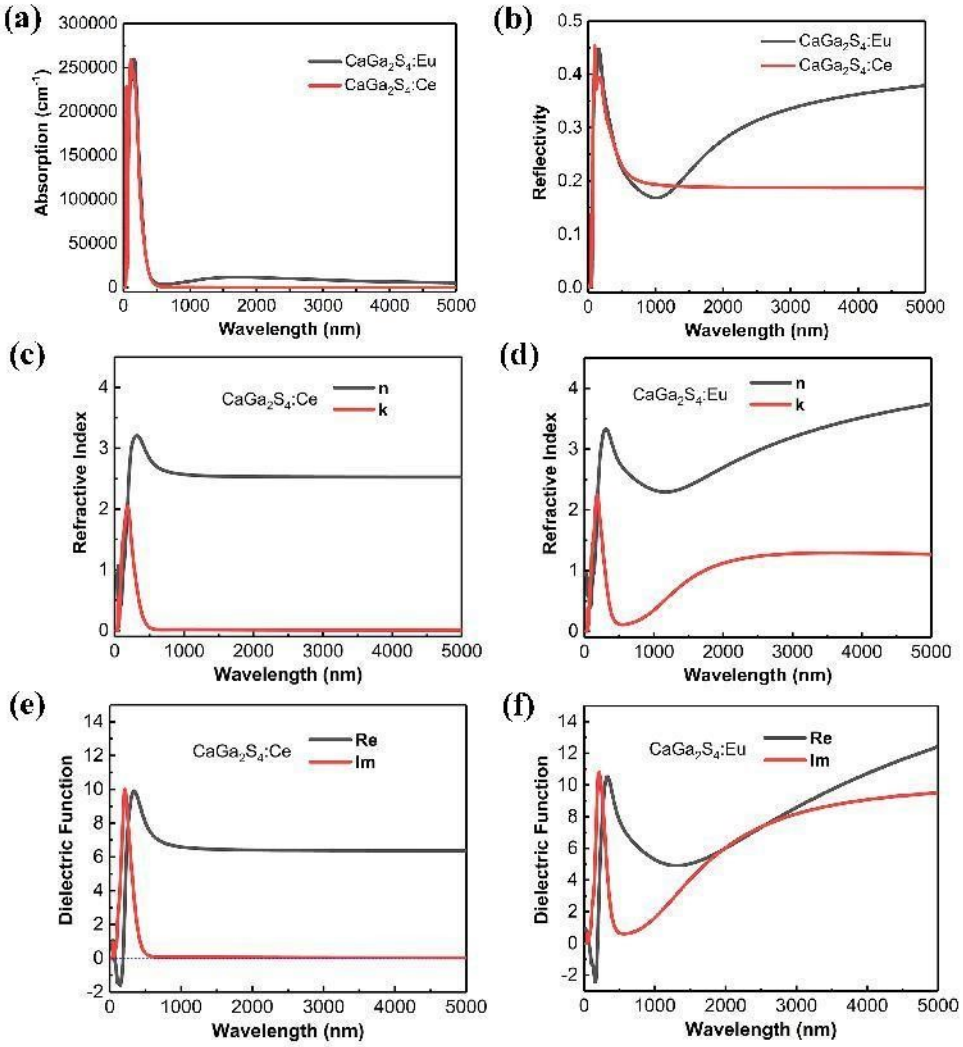

Fig. S13. The calculated dielectric functions and optical properties, i.e. reflectivity, refractive index and light absorption of $CaGa_2S_4$: Eu and $CaGa_2S_4$: Ce.

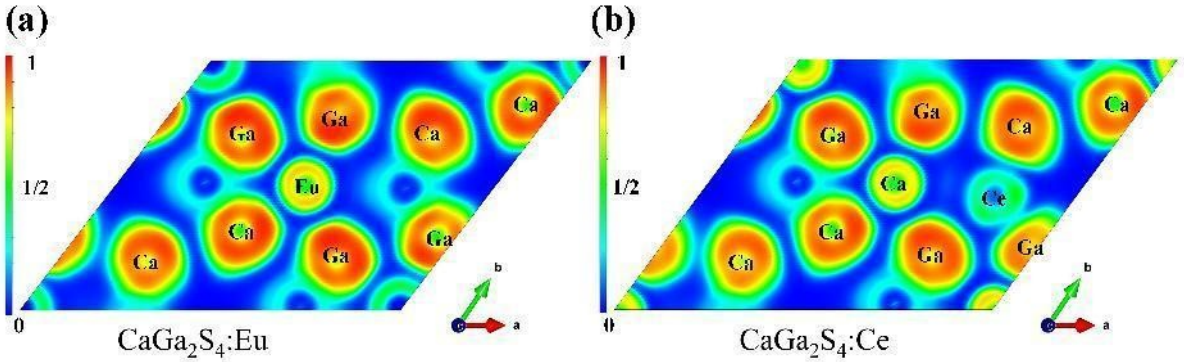

Fig. S14. The ELF maps of (a) $CaGa_2S_4$: Eu and (b) $CaGa_2S_4$: Ce, respectively.

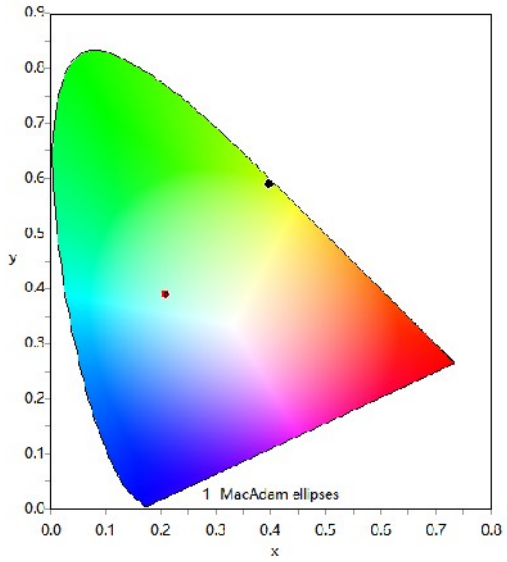

Fig. S15. CIE color coordinate diagram corresponding to PL spectrum of the Eu-$CaGa_2S_4$ and Ce-$CaGa_2S_4$.

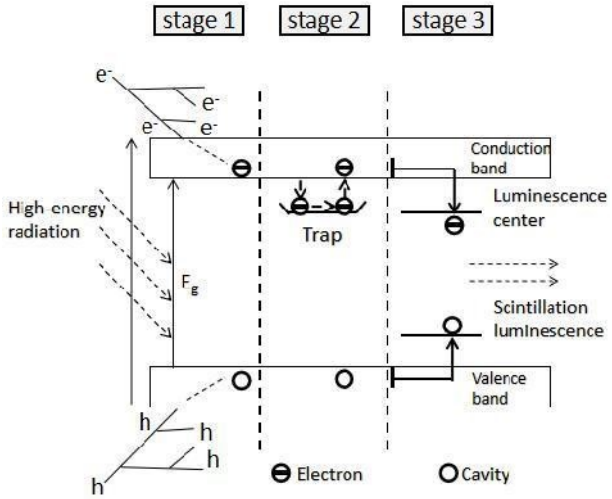

Fig.S16. Schematic diagram of scintillation mechanism.

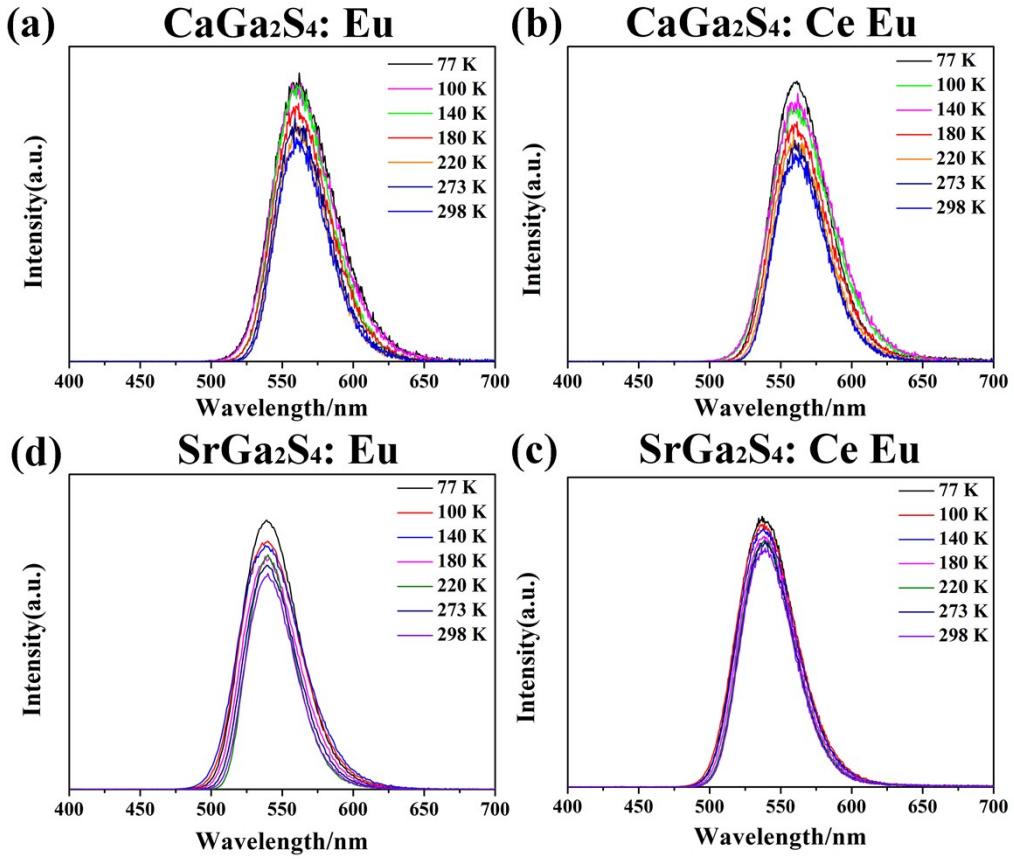

Fig.S17. Study on temperature-dependent photoluminescence of the Eu and Ce–Eu doped host $CaGa_2S_4$ and the Eu, Ce and Ce–Eu doped host $SrGa_2S_4$.

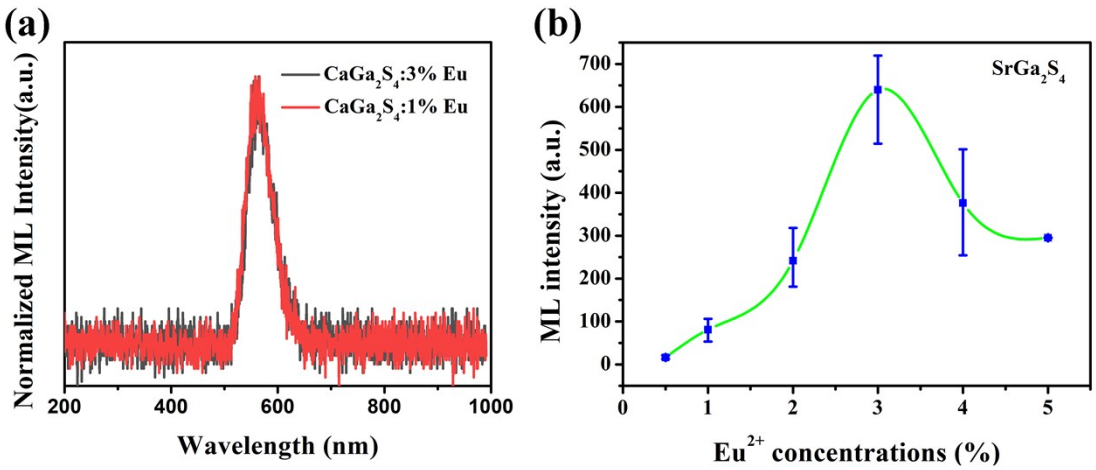

Fig. S18. Integrated ML emission comparison of the Eu-doped (a) $CaGa_2S_4$ and (b) $SrGa_2S_4$, respectively.

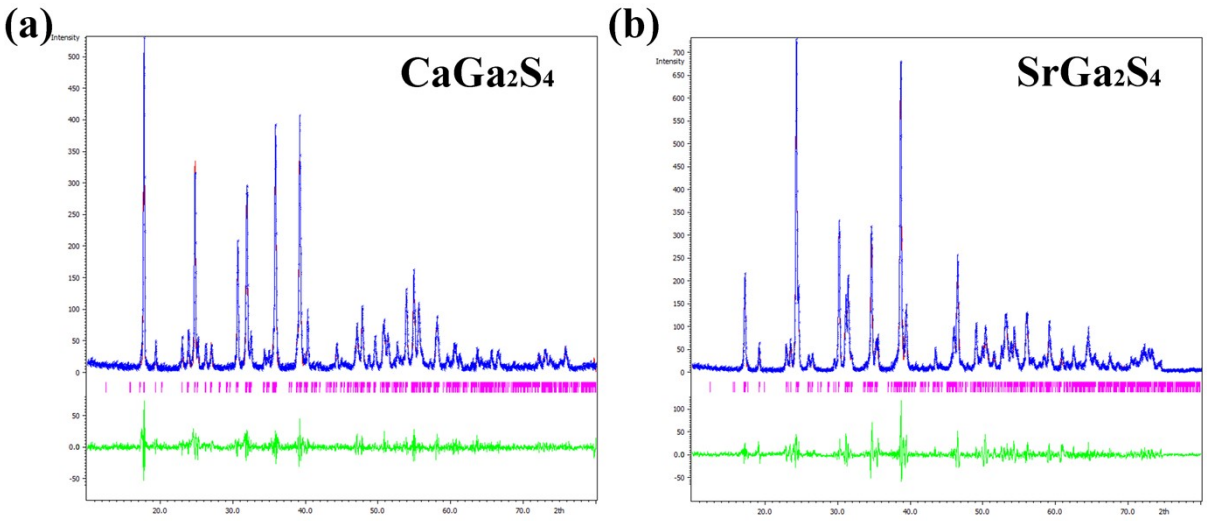

Fig. S19. Rietveld refinement of (a) $CaGa_2S_4$ and (b) $SrGa_2S_4$, respectively.